Study on the mechanical property of textile reinforced self-stressing concrete sheets

Article *in* Construction and Building Materials · March 2016

DOI: 10.1016/j.conbuildmat.2015.12.167

4 authors, including:

Boxin Wang
Jilin University
17 PUBLICATIONS **15** CITATIONS
SEE PROFILE

Teng Man
University of Minnesota Twin Cities
8 PUBLICATIONS **12** CITATIONS
SEE PROFILE

Construction and Building Materials 107 (2016) 1–10

Contents lists available at ScienceDirect

Construction and Building Materials

journal homepage: www.elsevier.com/locate/conbuildmat

Study on the mechanical property of textile reinforced self-stressing concrete sheets

Boxin Wang [a], Henan Jin [a,b], Teng Man [a,c], Qing Wang [a,*]

[a] Construction Engineering College, Jilin University, 130021 Changchun, Jilin, China
[b] Chang Chun Institute of Optics, Fine Mechanics and Physics, Chinese Academy of Sciences, 130033 Changchun, Jilin, China
[c] Department of Civil, Environmental, and Geo-Engineering, University of Minnesota, United States

HIGHLIGHTS

- Adopts textile reinforced self-stressing concrete (TRSSC) composite materials.
- Pull-out and bending tests of TRSSC sheets to gain better stress distribution of the bond behavior and bending property.
- The calculation formula of the bond strength is established based on Tepfers' partly cracked thick-walled cylinder model.
- Derivation of calculation models for TRSSC sheets elimination pressure moment.

ARTICLE INFO

Article history:
Received 19 August 2015
Received in revised form 3 December 2015
Accepted 22 December 2015

Keywords:
Textile
Self-stressing concrete
Sheets
Bond
Bend

ABSTRACT

This study tests the mechanical property of textile reinforced self-stressing concrete (TRSSC) sheets, particularly the bond behavior between fiber bundles and self-stressing concrete sheets and the bending property of a TRSSC one-way sheet under four-point loading to understand the enhancement mechanism associated with TRSSC. Bond test results show that the ultimate pull-out force increases with an increase in the initial bond length. The bond behavior between textiles and self-stressing concrete is superior to that between textiles and common concrete. The calculation formula of bond strength is established, and the bending test results show that the cracking load of the TRSSC sheets is greater than that of textile reinforced concrete (TRC) sheets. The cracking capacity and ultimate bearing capacity of TRSSC is analyzed, and the calculation results are congruent with the experimental results.

1. Introduction

Textile reinforced concrete (TRC) is characteristically corrosion resistant, anti-magnetic, and lightweight, and it can be used for certain special structures [1,2]. However, its load capacity significantly decreases at the concrete cracking point, and the debonding phenomenon occurs in the textile and matrix interface because of stress concentration. The crack behavior of TRC specimens depends on the bond behavior between the fiber bundles and the concrete. This study adopts a self-stressing concrete with a self-expansion behavior to improve the bond behavior in TRC. The self-expansion behavior is restrained by textiles in the hardening process and produces self-pressure, which can significantly improve the cracking load. The restrained matrix exerts a strong gripping, which significantly improves the bonding property. The enhancement mechanism of textile reinforced self-stressing concrete (TRSSC) is quite different from that of TRC because of the self-expansion behavior. Using the pull-out and four-point bending tests on the TRSSC sheets and the TRC specimens for comparison, this study discusses bond behavior and bending property. The micro-morphology of the bond interface between the textile and self-stressing concrete is observed through a scanning electron microscopy (SEM) test. The calculation formula of the bond strength is established based on Tepfers' partly cracked thick-walled cylinder model, and the bending mechanical behavior of TRSSC one-way sheets is calculated and analyzed.

2. Materials and experimental procedures

2.1. Materials

2.1.1. Textile

The textiles used in this experiment consisted of both the warp and weft made from alkali-resistant glass fibers using plain weaving methods. Given that epoxy resin greatly improves the synergistic ability of textiles [3,4], the surface of the fiber

* Corresponding author.
E-mail addresses: boxinwang@jlu.edu.cn (B. Wang), jinhenanking@126.com (H. Jin), manteng0520@gmail.com (T. Man), wangqing@jlu.edu.cn (Q. Wang).

http://dx.doi.org/10.1016/j.conbuildmat.2015.12.167
0950-0618/

Table 1
Property of alkali-resistant glass fiber.

Fiber type	Number of fibers	Tensile strength/MPa	Elastic modulus/GPa	Linear density/Tex	Theoretical area/mm^2
ARC13-2700H	9.2	1600	72	2700	0.975

Note: ARC13-2700H stands for alkali resistant continuous roving with fibrils diameter of 13 μm and linear density of 2700. *H* means that the content of ZrO_2 is more than 16%.

Table 2
Concrete mixture proportions.

Matrix	Cement/kg m^{-3}	Water/kg m^{-3}	Fine aggregate/kg m^{-3}	Coarse aggregate/kg m^{-3}	Super plasticizer/kg m^{-3}
SSC1	663	239	796	530	1.19
SSC2	625	281	500	750	0.93
C	663	239	796	530	1.19

Note: Self-stressing cement units were more than 550 kg m^{-3} because the SSC mix is designed to withstand a large self-stress value. This comprehensive consideration is based on the expansion property and mixture performance.

Table 3
Mechanical property of the matrix.

Matrix type	Compressive strength of 28d/MPa	Flexural strength of 28d/MPa	Free expansion rate/10^{-6}		
			7d	21d	28d
SSC1	33	8.46	11,435	13,856	14,201
SSC2	35	7.83	6198	7620	7733
C	47	5.28	1125	250	−875

Note: The curing conditions for three types of mixes is 20 ± 2 °C, and the humidity is over 95%. The free expansion rate of 28 d is negative because of the common concrete contraction process after the expansion in the process of hydration.

bundle was impregnated with epoxy resin to ensure that the fibers have strong synergistic force. Each textile grid had a space of 20 mm or 40 mm; the specific material parameters are shown in Table 1.

2.1.2. Self-stressing concrete

The traditional mix ratio of self-stressing concrete must be optimized to improve the bonding behavior of textiles and self-stressing concrete. Given the small mesh size of the textile, the maximum grain size of coarse aggregates cannot be larger than 16 mm. The flow ability of the matrix must be improved to ensure that the concrete fully warps the textiles. Self-stressing cement uses level-4 safety self-stressing cement [5]; Common cement uses P.O.42.5 cement. Three kinds of concrete mixes are shown in Table 2 [6]. The common concrete mix was used for the comparison test. The mix of SSC1 and C was used for the bond test, and that of SSC1, SSC2, and C was used for the four-point bending test. The physical and mechanical property of the three kinds of matrices is shown in Table 3.

2.2. Experimental procedures

2.2.1. Bond test

The ability of textiles and self-stressing concrete to coordinate with each other is dependent on the bond behavior. Pull-out tests can realistically reflect the stress distribution of the bond surface when a structure bears loads [7]. Pull-out tests examine the influence of the initial bond length of a textile and the matrix on bond behavior, thereby allowing the comparison of the common concrete matrix specimens. The size of clamping fixture was designed with 50 mm to eliminate the influence of the clamp part of the bond test. First, the wooden molds of 800 mm × 400 mm × 20 mm and 800 mm × 400 mm × 15 mm are made. The mold with the cover thickness is first made, and the textile is fixed on it, and the remaining part of the mold is installed. The concrete is poured into the molds with the slight vibration. The test sheets were sawn from 200 mm × 80 mm × 20 mm and 200 mm × 80 mm × 15 mm plate after the standard curing condition for 28 days.

The bond test was conducted on eight groups, each of which contained five specimens (Table 4). The pull-out specimen for each cutting seam was reserved as the fiber bundle. The electronic universal testing machine was used for loading at a rate of 1.0 min/mm [8]. The load–displacement curve was obtained through the Germany IMC dynamic testing system (Fig. 1).

2.2.2. Four-point bending test

The test sheet was sawn from a 400 mm × 120 mm × 20 mm metal plate. The textile was laid at cover thickness distance from the bottom surface. The bending test specimens were tested in nine groups, and each group consisted of four specimens (Table 5). The electronic universal testing machine was used to apply the load; the four-point bending test device is shown in Fig. 2. Load and displacement sensors determine the load and span deflections. The load–displacement curve is collected by the Germany IMC dynamic testing system. The loading method is displacement control, and the loading rate is 0.3 mm/min [9]. Test is stopped when the curve peak decreases significantly, or the first fiber bundle fractures (Fig. 3).

Table 4
Groups of specimens.

Matrix type	Thickness/mm	Bond length/mm	Cover thickness/mm
SSC1(C)	15	20	7
		30	7
		40	7
		50	7
	20	20	10
		30	10
		40	10
		50	10

3. Results and discussions

3.1. Bond behavior

3.1.1. Effect of fiber bond length on bond behavior

The ultimate pull-out force increases when the initial bond length is enhanced (Fig. 4). The friction resistance between the fiber bundle and the self-stressing concrete is more serious because of the longer bond length and larger contact area with the matrix than those of between the fiber bundle and the common concrete. When the embedded fiber bundle length is less than 30 mm, the fiber bundle can be slowly pulled out from the specimen (Fig. 5a). The surface of the fiber bundle displays wear condition. When the embedded fiber bundle length is more than 40 mm, the curve appears to drop steeply (Fig. 5b). This finding indicates that the fiber bundle cannot bear the load when the internal parts of the fibers reach the ultimate load. During this process, a very clear fracture sound occurs during the pull out.

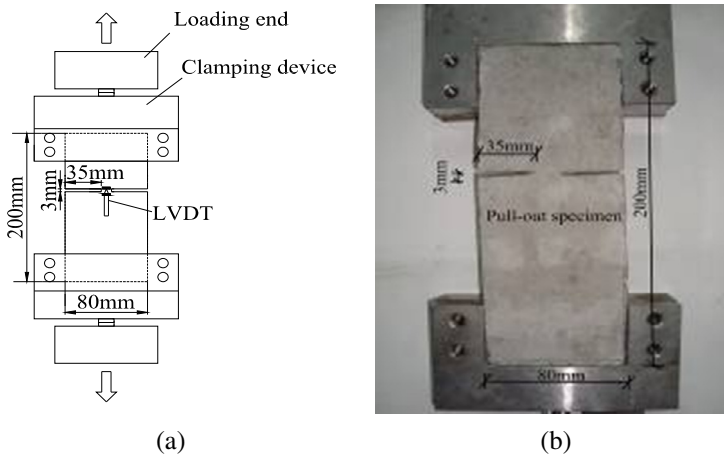

Fig. 1. Details of the pull-out test: (a) loading setup and (b) grips and specimen.

Table 5
List of specimens.

Matrix type	Specimen number	Cover thickness/mm	Number of fibers	Mesh size
SSC1	S1-3-A	3	18.4	40 × 40
SSC2	S2-3-A	3	18.4	40 × 40
SSC1	S1-3-B	3	9.2	40 × 40
SSC2	S2-3-B	3	9.2	40 × 40
SSC1	S1-3-C	3	9.2	20 × 20
SSC2	S2-3-C	3	9.2	20 × 20
C	C-3-A	3	18.4	40 × 40
SSC1	S1-8-A	8	18.4	40 × 40
SSC2	S2-8-A	8	18.4	40 × 40

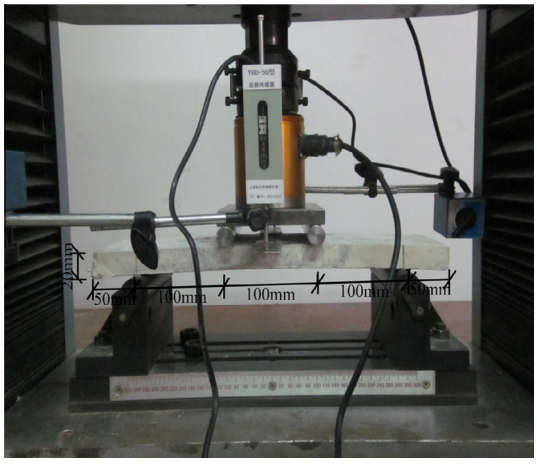

Fig. 2. Four-point bending test.

3.1.2. Effect of the matrix type of ultimate pull-out force and energy dissipation capacity

When the directional fiber bundle bond length is the same, the ultimate pull-out force and energy dissipation capacity of the self-stressing concrete matrix specimens are significantly greater than that of the common concrete matrix specimens (Fig. 6). The ultimate pull-out force of self-stressing concrete matrix specimens is higher than that of the common concrete matrix specimens by 9–27% (Table 6), and the energy dissipation capacity of the self-stressing concrete matrix specimens is higher than that of the common concrete matrix specimens by 16–48% (Table 7). The self-expansion behavior of the self-stressing concrete produces self-stress because the textile in the hardening process restrains it. The expansion of the self-stressing concrete produces radial compressive stress on the fiber bundle, which increases the ultimate pull-out force and the energy dissipation capacity. The bond behavior between the textile and self-stressing concrete is superior to that between the textile and common concrete.

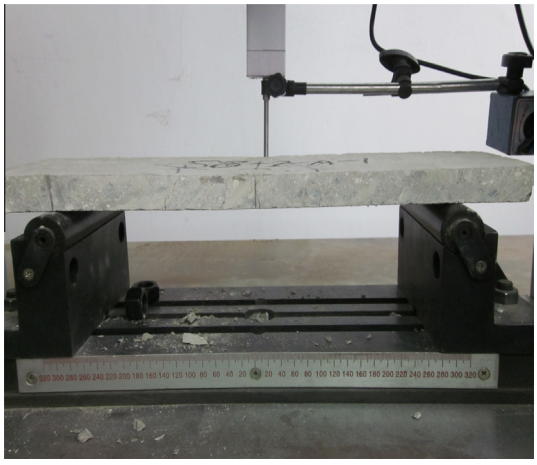

Fig. 3. Sheet specimen after loading.

3.1.3. Theoretical models of the bond strength between the fiber bundle and self-stressing concrete

The calculation formula of the bond strength of reinforced concrete is derived from the experimental data regression [10–12]. Although these calculation formulas can reflect the bond strength to a certain extent, the test is often on a specific concrete material so that the scope of its application is limited. The calculation model of bond strength under the friction effect is obtained in this study based on Tepfers' partly cracked thick-walled cylinder model [13].

The pull-out specimens can be analyzed using the method of elastic mechanics as the thick-walled cylinder model under the pressure distribution. The diagram of self-stressing concrete within the scope of the unit length of the fiber bundle is shown in Fig. 7. P is the constraint force between the fiber bundle and self-stressing concrete; μP is the friction effect between the fiber bundle and self-stressing concrete; the radial force is the uniform pressure P_1 of the self-stressing concrete; and the longitudinal force is the bond strength τ between the fiber bundle and self-stressing concrete. τ and P_1 are calculated using Eq. (1).

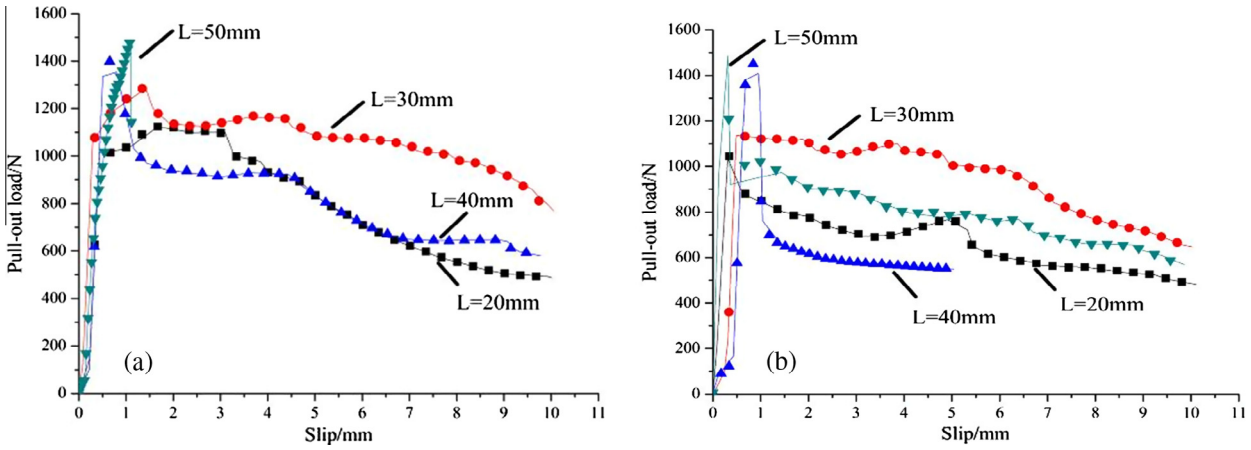

Fig. 4. Influence of the initial bond length on the bond between textile and self-stressing concrete: (a) plate thickness of 15 mm and (b) plate thickness of 20 mm.

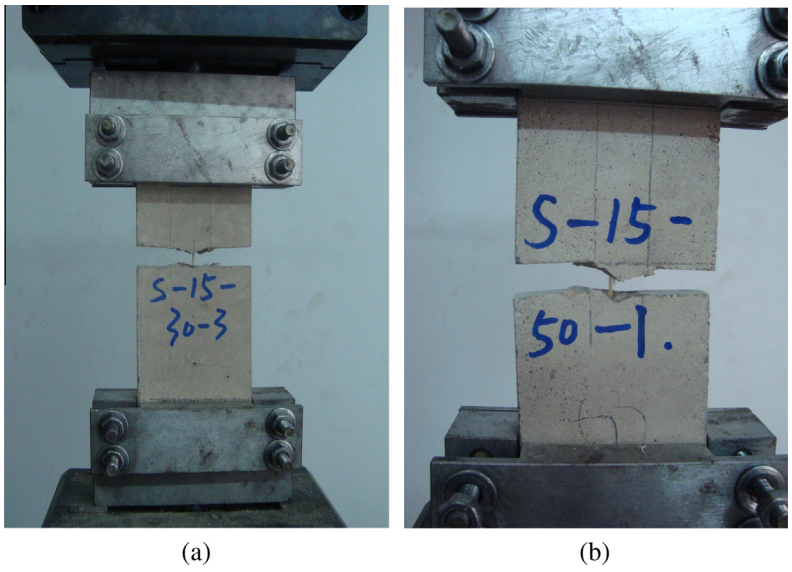

Fig. 5. Results of the pull-out test for the fiber bundle: (a) pull-out failure and (b) tensile failure.

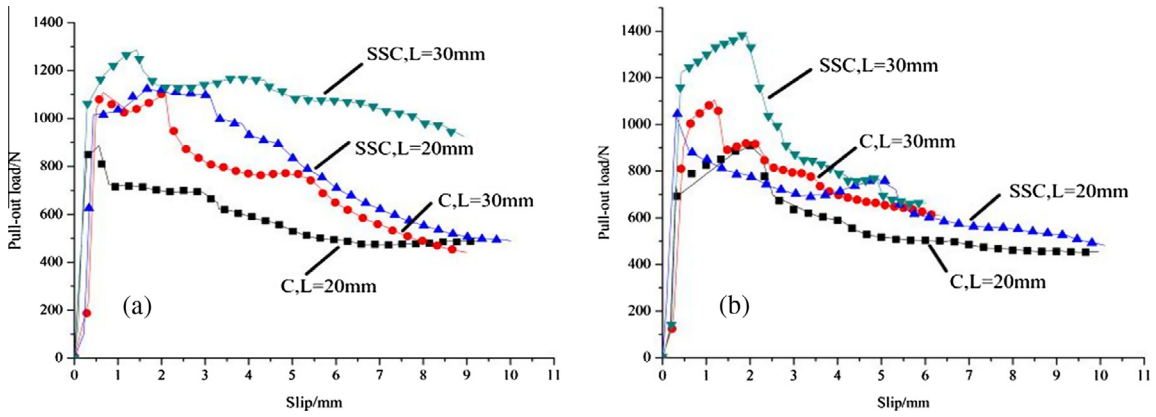

Fig. 6. Influence of the matrix on the bonding between textile and matrix: (a) plate thickness of 15 mm and (b) plate thickness of 20 mm.

$$\tau = \mu P, \quad P_1 = P \tag{1}$$

Tension specimens use the elastic model of partly cracked thick-walled cylinder (Fig. 8). P_2 is the compressive stress of the part of the self-stressing concrete that does not undergo cracking. According to the elastic mechanics,

$$P_1 \pi d = 2b\pi P_2 \tag{2}$$

where d is the diameter of the fiber bundle, and b is the distance from the center of the fiber bundle to the edge of the cracked concrete.

Table 6
Comparison of the ultimate pull-out force results.

Specimen thickness/mm	Bond length	Results		
	l_a/mm	$F_{SSC,M}$/N	$F_{C,M}$/N	$F_{SSC,M}/F_{C,M}$
D = 15	20	1127.74	888.52	1.27
	30	1287.05	1087.01	1.18
	40	1399.16	1281.55	1.09
	50	1490.0	1326.50	1.12
D = 20	20	1053.28	911.57	1.16
	30	1383.13	1106.90	1.25
	40	1435.81	1209.50	1.19
	50	1488.04	1314.31	1.13

Note: $F_{SSC,M}$ is the ultimate pull-out force of the self-stressing concrete matrix specimens, and $F_{C,M}$ is that of the common concrete matrix specimens.

Table 7
Comparison of the energy dissipation capacity results.

Specimen thickness/mm	Bond length	Results		
	l_a/mm	S_{SSC}/N mm	S_C/N mm	S_{SSC}/S_C
D = 15	20	7876.44	5376.76	1.46
	30	9651.93	6521.69	1.48
D = 20	20	6684.15	5744.54	1.16
	30	5583.20	4763.54	1.17

Note: S_{SSC} is the area under the load–displacement curve of the self-stressing concrete matrix specimens, and S_C is that of the common concrete matrix specimens.

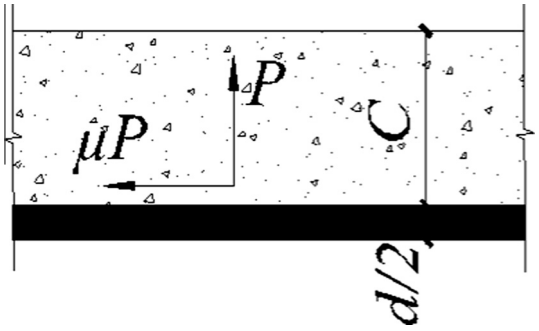

Fig. 7. Stress unit of self-stressing concrete.

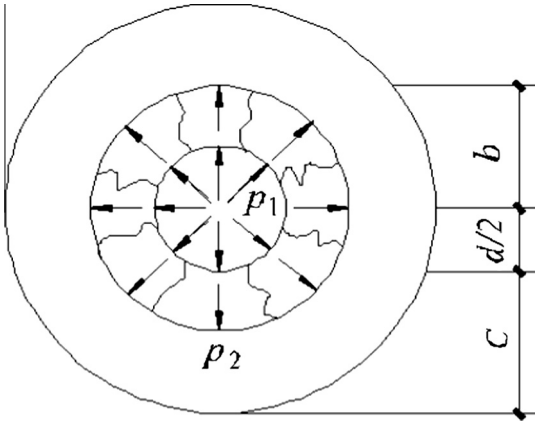

Fig. 8. Mechanical model of partly cracked concrete.

The non-cracked part of the self-stressing concrete is equivalent to the thick-walled cylinder with the effect of uniform internal pressure P_2. The circumferential tensile stress is calculated by Eq. (3) [14]:

$$\sigma_\theta = \frac{b^2 P_2}{(c+d/2)^2 - b^2}\left[1 + \frac{(c+d/2)^2}{r^2}\right] \tag{3}$$

where C is the protective layer thickness of the fiber bundle, and r is the distance from the center of the specimen to any point on the specimen.

The inner radius of the cracking concrete is $d/2$, and the outer radius is b. The biggest circumferential tensile stress of the non-cracked concrete should be located at $r = b$. Inserting $r = b$ in Eq. (3) and considering Eqs. (1) and (2), the calculation of $\sigma_{\theta\max}$ can be expressed by Eq. (4):

$$\sigma_{\theta\max} = \frac{Pd}{2b}\frac{(c+d/2)^2 + b^2}{(c+d/2)^2 - b^2} \tag{4}$$

The cracking strength of the self-stressing concrete is given by Eq. (5):

$$\sigma_{\theta\max} = f_{cr} \tag{5}$$

By inserting Eq. (5) in Eq. (4), the following expression can be obtained:

$$\frac{p}{f_{cr}} = \frac{2b}{d}\frac{(c+d/2)^2 - b^2}{(c+d/2)^2 + b^2} \tag{6}$$

The maximum cracking radius $b_{\max}$ can be obtained by Eq. (6) and expressed by Eq. (7):

$$b_{\max} = 0.486(c+d/2) \tag{7}$$

By inserting Eq (7) in Eq (6), the maximum of P, which is given by the following function, can be obtained:

$$p = \frac{c+d/2}{1.664d} f_{cr} \tag{8}$$

By inserting Eq. (8) in Eq. (1), the following bond strength formula can be obtained:

$$\tau = \mu\frac{c+d/2}{1.664d} f_{cr} \tag{9}$$

The calculation formula of bond strength considers the cracking strength of the self-stressing concrete and the friction coefficient of the bond interface between the fiber bundle and self-stressing concrete, where f_{cr} is related to the limited expansion volume of the self-stressing concrete and μ is the undetermined constant. The bond test results show that the bond behavior between textile and self-stressing concrete is superior to that of the textile and common concrete. Therefore, μ is related not only to the fiber surface roughness, but also to the tight wrapping of the self-stressing concrete on fiber bundle.

The test for directly measuring the friction coefficient is very difficult to conduct because many factors influence the friction coefficient. The value of the friction coefficient can be derived through the statistical analysis of the test data and by considering Eq. (9). The μ value of the bond interface between the fiber bundle and self-stressing concrete is 0.93, and the μ value of the bond interface between the fiber bundle and common concrete is 0.88.

3.1.4. Analysis of the electron microscopy test

3.1.4.1. Micro-morphology of the matrix. The test adopts the JSM-6700 field emission SEM to observe the micro-morphology of the matrix. The hydration minerals of sulpho-aluminate expansion cement mainly includes ettringite (Aft), hydration alumina gel ($Al_2O_3{\cdot}3H_2O$), and hydration calcium silicate gel (C–S–H). The fundamental cause of sulpho-aluminate expansion is the formation of Aft. Aft is an acicular or hexagonal columnar crystal that produces a significant volume expansion in its dense internal structure [15]. The expansion turns to self stress under restricted conditions

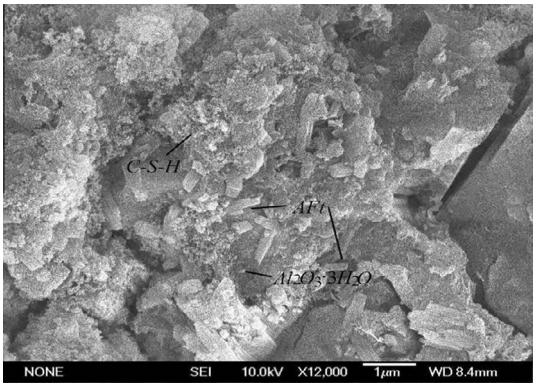

Fig. 9. SEM photograph of the self-stressing concrete matrix.

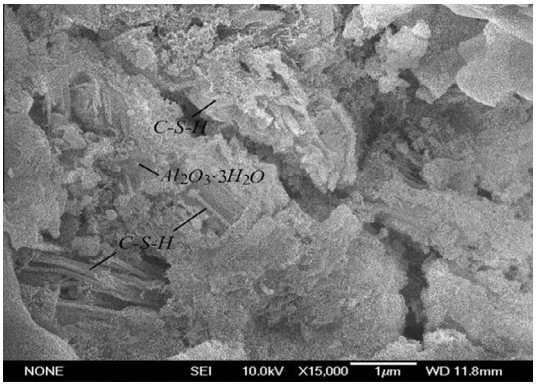

Fig. 10. SEM photograph of the common concrete matrix.

because of the crystallization pressure in the process of hydration and hardening. No essential difference exists in the main hydration products of expansion cement and common concrete. The expansion of cement is caused by the crystallization pressure of Aft crystals; thus, the quantity of the Aft crystals of expansion cement is much more than that of common cement. The quantity of the Aft crystals is high (Fig. 9), but finding an acicular or hexagonal columnar crystal is difficult (Fig. 10). The self-stressing concrete matrix is denser than common concrete matrix because the Aft crystals are constrained by the textile in the process of formation. The fiber wrapped tightly between the fiber bundle and self-stressing concrete is far higher than that between the fiber bundle and common concrete, which improves the μ value and greatly enhances bond behavior. The expansion deformation of self-stressing concrete

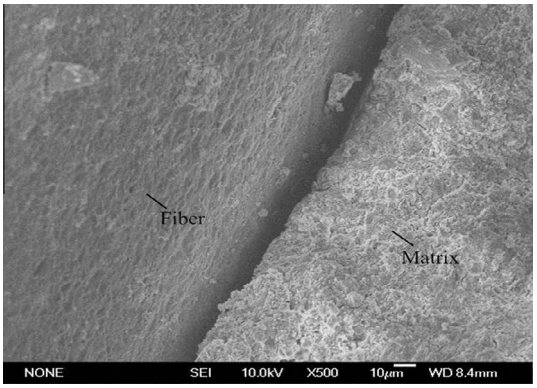

Fig. 11. SEM photograph of the fiber surface before the pull-out test.

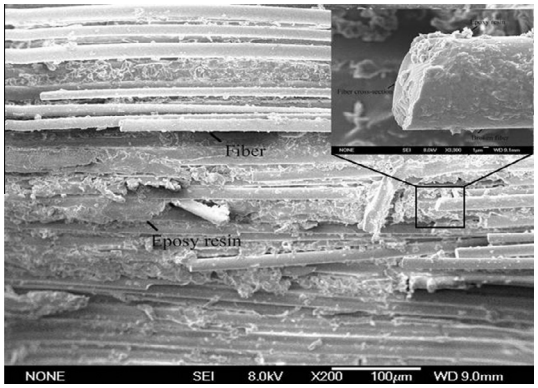

Fig. 12. SEM photograph of the fiber surface after the pull-out test.

turns to self stress under the textile restriction, which leads to the higher f_{cr} value of the self-stressing concrete matrix specimens than that of the common concrete matrix specimens.

3.1.4.2. Micro-morphology of the fiber bundle. The fiber surface is not broken and is coated well by epoxy resin (Fig. 11). The external part of the fiber is broken (Fig. 12). Some signal fiber monofilaments reaches the ultimate strength and break because of the tight bond between the external part of the fiber bundle and self-stressing concrete, which causes severe damage to the external surface of fiber bundle. The broken position is obviously different, which indicates that the stress level of the fiber bundle is not the same, although the bundle is impregnated by epoxy resin. The monofilament amplification of the SEM photo shows that, although the stress degrees among the fiber monofilaments differ, the surface wear of the fiber monofilament is not serious. The tensile stress exceeds the tensile strength, thereby causing the fiber to break; the fracture is even.

3.1.4.3. Micro-morphology of the bond interface between the fiber bundle and concrete. The bond interface damage of the self-stressing concrete matrix (Fig. 13) is more serious than that common concrete matrix (Fig. 14). The epoxy resin particles from the fiber bundle surface (Fig. 13) are smaller and more dispersed than that in Fig. 14. The surface of the epoxy resin-impregnated fiber bundle is uneven and has many small cavities. The expansion stress forces hydrates to penetrate these small cavities in the process of self-stressing concrete hydration, and the bond between the hydrates and the surface of fiber bundle becomes increasingly dense, so that the mechanical interlocking effect fully assumes

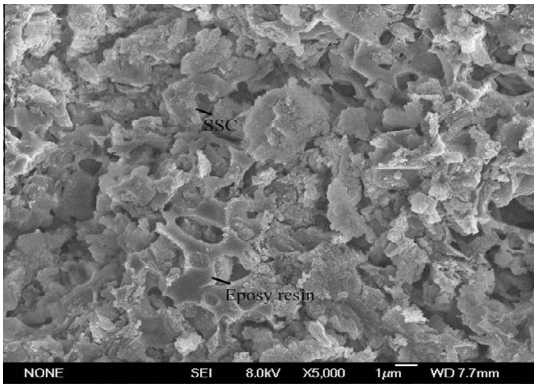

Fig. 13. SEM photograph of the bond interface between fiber and self-stressing concrete.

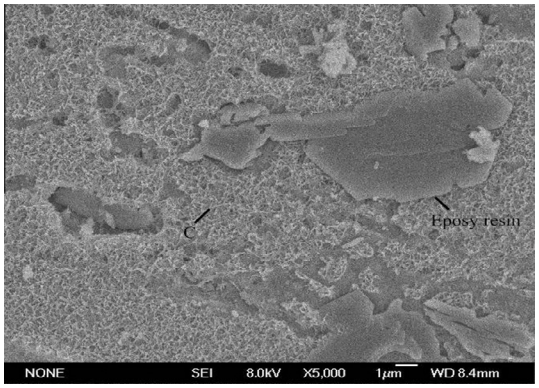

Fig. 14. SEM photograph of the bond interface between fiber and common concrete.

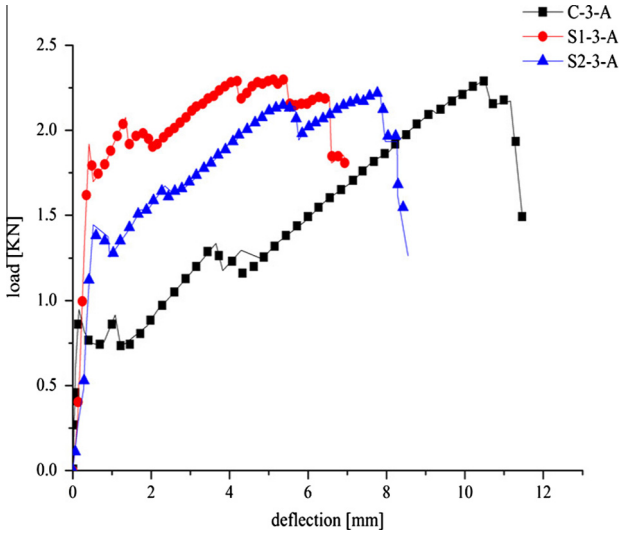

Fig. 15. Influence of the common and self-stressing concrete matrices on slab bending.

the role of increasing the μ value to greatly enhance the bond strength between the fiber bundle and self-stressing concrete. The existence of increasingly large mechanical interlocking force results in the significant destruction of the original dense matrix in the pull-out process. Thus, the bond behavior between the textile and self-stressing concrete is superior to that between the textile and common concrete.

The microscopic points above show the existence of a large number of Aft crystals. The expansion deformation of the self-stressing concrete turns to self stress under textile restrictions; thus, the f_{cr} value of self-stressing concrete becomes greater than that of common concrete. The volume expansion of self-stressing concrete increases the density of the fiber bundle wrap. As a result, the friction coefficient of the bond interface between fiber bundle and self-stressing concrete becomes larger than that of the bond interface between fiber bundle and common concrete. The bond behavior between the textile and self-stressing concrete is superior to that between the textile and common concrete, which agrees with the experimental results.

3.2. Bending property

3.2.1. Influence of the matrix type on sheet bending property

The cracking load of the TRSSC sheet is significantly greater than that of the TRC sheet (Fig. 15, Table 8). The cracking load of the TRSSC sheet can reach 1.93 KN, whereas that of the TRC sheet is only 0.95 KN, because self-stressing concrete hydration products include a large number of Aft crystals. The volume expansion of Aft crystals is limited by the fiber bundle, which produces pre-stress and improves the cracking load of the bending sheet specimens. Furthermore, the cracking load of the SSC1 mix proportion is larger than that of the SSC2 mix proportion because the self-stressing cement dosage of the SSC1 mix proportion is more than that of the SSC2 mix proportion; thus, more Aft crystals are found in the former than in the latter (Table 8). Under the same restrictions, the self-stress value and cracking load of the specimen increase with an increase in the limited expansion ratio of the SSC1 specimens. The limited expansion is not uniform because the cover thickness of the self-stressing concrete is thin and the textile is close to the bottom of the specimen. As a result, an inner arch appears, which becomes more obvious with more free expansion in the self-stressing concrete specimens. Self-stressing concrete sheet specimens must first cancel the inner arch effect in the early-loading stage, so that the cracking deflection of the TRSSC sheet specimens is greater than that of the TRC sheet specimens. The ultimate loads of the three groups differ only slightly because the pre-stress of self-stressing concrete does not improve the ultimate bearing capacity (Fig. 15).

Table 8
Results of the bending tests.

Specimen number	Cracking deformation/mm	Cracking load/kN	Ultimate load/kN	Limited expansion ratio/10^{-6}	Self stress value/MPa
S1-3-A	0.42	1.92	2.31	6075	1.07
S2-3-A	0.51	1.44	2.23	5325	0.89
S1-3-B	0.28	1.50	1.61	7750	0.67
S2-3-B	0.21	1.46	1.52	6625	0.58
S1-3-C	0.43	1.93	3.32	4525	0.81
S2-3-C	0.35	1.80	3.64	4075	0.71
C-3-A	0.16	0.95	2.30	...	...
S1-8-A	0.35	1.71	1.84	5525	0.98
S2-8-A	0.32	1.34	1.70	4825	0.85

3.2.2. Influence of distribution textile rate on the bending property of TRSSC sheet

The influence of the distribution textile rate on the bending property of the TRSSC sheet is explored using a number of fiber bundles and mesh sizes (Fig. 16, Table 8). For both the SSC1 and SSC2 mix proportions, the total cracking deflection, cracking load, and ultimate load increase with an increase in textile distribution rates. Increasing the number of fiber bundles is one mechanism of improving the distribution textile rate. A large rate increases the restricted expansion of the TRSSC specimen and improves the self-stress value. The cracking deflection and load eventually increase with an increase in the self-stress value and inner arch. At the same time, increasing the distribution rate can improve the ultimate load. The distribution rate of the S1-3-A specimen is twice that of the S1-3-B specimen. The self-stress value, cracking deflection, cracking load, and ultimate load increase by 37%, 33%, 32%, and 30%, respectively.

3.2.3. Influence of cover thickness on sheet bending property

The cracking deflection, cracking load, and ultimate load increase with a decrease in cover thickness (Fig. 17, Table 8). The cracking deflection, cracking load, and ultimate load increase by 37%, 13%, and 24%, respectively, relative to those of specimen S2-8-A. The textile has a strong limitation on a certain radius of the concrete in the process of restricted expansion because the textile is not uniformly distributed in the concrete. An increase in the

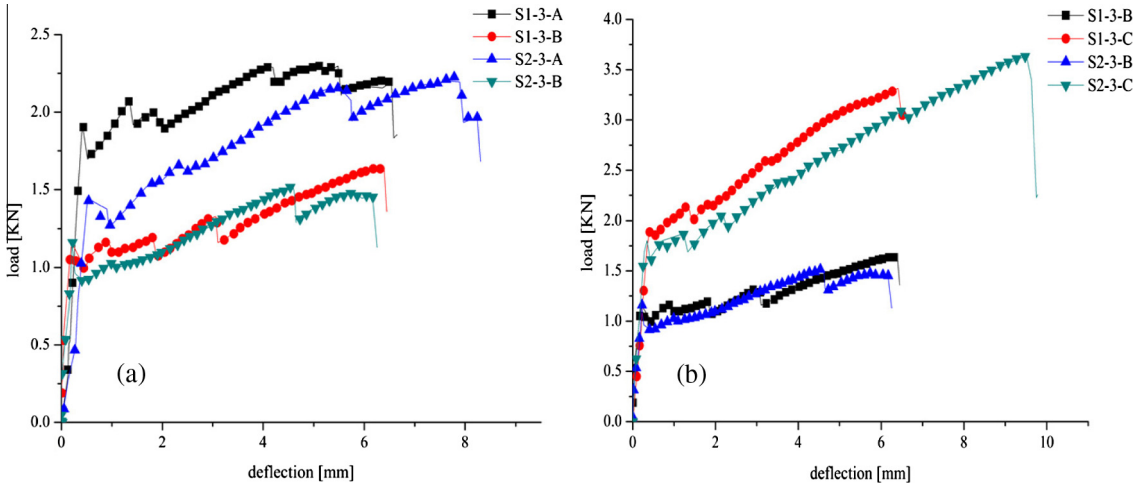

Fig. 16. Influence of the distribution textile rate on slab bending: (a) number of fibers of 9.2 and 18.4 and (b) grid size of 20 mm and 40 mm.

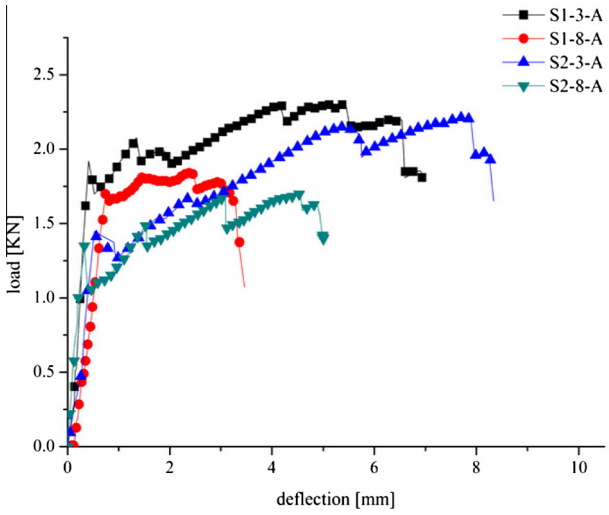

Fig. 17. Influence of the protective layer of 3 mm and 8 mm.

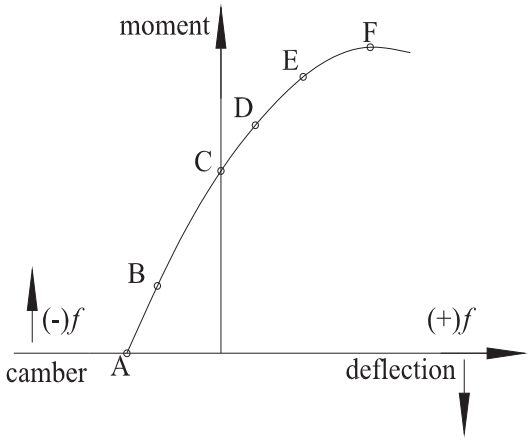

Fig. 18. Curve of the load vs. the displacement of the TRSSC beam.

cover thickness gradually weakens the limitation and decreases the cracking deflection and cracking load. A decrease in cover thickness increases both the effective section height and ultimate load.

3.2.4. Analysis of the bending mechanical property of the TRSSC sheet

The loading process of the TRSSC beam differs from that of the TRC beam, but the damage is similar because of pre-stress. The entire loading process can be divided into two stages (Fig. 18).

The physical meanings of points A, B, C, D and E are releasing pressure, eliminating tension stress, de-compression, section cracking and section failure.

Stage 1: The curve of the AE segment is obtained by applying the load to the appearing cracks. The AE segment is divided into the upper edge concrete eliminating pull stage AB, eliminating arch stage BC, the lower edge concrete de-compression stage CD, and the section cracking stage DE. If self stress leads to surface pressure, the AB stage is not necessary before loading.

Stage 2: The curve of the EF segment is derived from section cracking to concrete crushing or textile breaking. Assuming that the sheet is loading, the cross-section deformation is still in accordance with the plane section assumption, and the calculation principle of the normal section bearing capacity of the reinforced concrete beam can be used for the TRC beam [16]. However, the TRSSC specimens include additional property beyond those associated with the basic TRC process, thereby increasing the complexity of the ultimate load calculation of TRSSC beam bending, which considers not only the equilibrium equations of force and moment but also the geometric equations of the section deformation.

The test sheet length to width ratio of the one-way slab is 3.3. The class-A and class-B TRSSC sheets can be regarded as three parallel beams with a cross section of 40 mm × 20 mm. Without considering the interaction between the beams, the force of the three beams is equal to the sheet force. The class-C TRCC sheets can be regarded as six parallel beams with a cross section of 20 mm × 20 mm. Without considering the interaction between the beams, the force of the six beams is equal to the sheet force.

The main damages to the TRSSC beam include crushed concrete and broken textile because the balance failure probability is small. All the test failures are textile breaks; thus, this study considers only textiles that are broken prior to the crushing of concrete. At this point, the compressive strain of the self-stressing concrete compressive region does not reach the ultimate compressive strain, and the equivalent coefficients α and β cannot be directly selected in accordance with the specifications. The equivalent coefficients α and β are calculated by Eqs. (10) and (11) [17]:

$$\alpha = \begin{cases} \left(\frac{\varepsilon_{ssc}}{\varepsilon_0} - \frac{\varepsilon_{ssc}^2}{3\varepsilon_0^2}\right)\frac{1}{\beta}, & 0 < \varepsilon_{ssc} \leqslant \varepsilon_0 \\ \left(1 - \frac{\varepsilon_0}{3\varepsilon_{ssc}}\right)\frac{1}{\beta}, & \varepsilon_0 < \varepsilon_{ssc} \leqslant \varepsilon_{cu} \end{cases} \quad (10)$$

Table 9
Values of equivalent coefficient α and β.

Compressive strain ε_{ssc}	0.0005	0.0006	0.0007	0.0008	0.0009	0.0010	0.0011	0.0012
α	0.275	0.324	0.371	0.416	0.460	0.501	0.540	0.577
β	0.679	0.681	0.684	0.687	0.689	0.692	0.695	0.698
Compressive strain ε_{ssc}	0.0013	0.0014	0.0015	0.0016	0.0017	0.0018	0.0019	0.002
α	0.613	0.646	0.678	0.707	0.735	0.761	0.785	0.807
β	0.702	0.705	0.708	0.712	0.716	0.719	0.723	0.727
Compressive strain ε_{ssc}	0.0021	0.0022	0.0023	0.0024	0.0025	0.0026	0.0027	0.0028
α	0.827	0.845	0.862	0.876	0.889	0.900	0.909	0.918
β	0.731	0.736	0.740	0.745	0.750	0.755	0.760	0.765
Compressive strain ε_{ssc}	0.0029	0.003	0.0031	0.0032	0.0033			
α	0.925	0.931	0.937	0.942	0.946			
β	0.771	0.776	0.781	0.785	0.790			

$$\beta = \begin{cases} \frac{4\varepsilon_0 - \varepsilon_{ssc}}{6\varepsilon_0 - 2\varepsilon_{ssc}}, & 0 < \varepsilon_{ssc} \leqslant \varepsilon_0 \\ 2 - \frac{6\varepsilon_{ssc}^2 - \varepsilon_0^2}{6\varepsilon_{ssc}^2 - 2\varepsilon_{ssc}\varepsilon_0}, & \varepsilon_0 < \varepsilon_{ssc} \leqslant \varepsilon_{cu} \end{cases} \tag{11}$$

In the above equations, ε_{ssc} is the self-stressing concrete compressive strain, ε_0 is the self-stressing concrete compressive strain corresponding to the peak stress, and ε_{cu} is the self-stressing concrete ultimate compressive strain.

First, two extreme-pressure strain values of the self-stressing concrete compressive edge are selected, and the corresponding equivalent coefficients α and β are derived (Table 9).

The height of the compressive zone x_0 is determined by the section assumption geometric Eq. (12):

$$x_0 = \frac{\varepsilon_{ssc}}{\varepsilon_{ssc} + \varepsilon'_{fu}} h_0 \tag{12}$$

where h_0 is the distance from the point of the tensile force to the section compression edge and ε'_{fu} is the tensile strain of the fiber bundle. Because of the bond stress effect of the fiber bundle and the self-stressing concrete, the fiber bundle is the stretched ε value, which is determined from the limited expansion ratio. Thus, from the loading up to the breaking of the fiber bundle, the elongated length of the fiber bundle is calculated using Eq. (13):

$$\varepsilon'_{fu} = \varepsilon_{fu} - \varepsilon \tag{13}$$

ε_{fu} is the ultimate tensile strain of the fiber bundle.

The balance equation of the force is given by the following function according to Fig. 19:

$$x_0 = \frac{nE_f\varepsilon'_{fu}A_f}{\alpha f_{ssc} b\beta} \tag{14}$$

where x_0 is the height of the compressive zone, n is the number of textile warp fiber bundles, E_f is the tensile elastic modulus of the warp fiber bundle, ε'_{fu} is the tensile strain of the fiber bundle, A_f is the theory section area of the single fiber bundle, f_{ssc} is the compressive strength of the self-stressing concrete matrix, b is the beam section width, and α and β are the equivalent coefficients.

If the results of Eqs. (12) and (14) are different, the dichotomy is used to readjust the ε_{ssc} value until the equations are approximately equal.

After obtaining the x_0, the ultimate bearing capacity M_u of the TRSSC beam can be expressed as Eq. (15) [18]:

$$M_u = \alpha f_{ssc}\beta x_0 b(h_0 - \beta x_0/2) \tag{15}$$

The cracking moment M_{cr} of the TRSSC beam is expressed by Eq. (16):

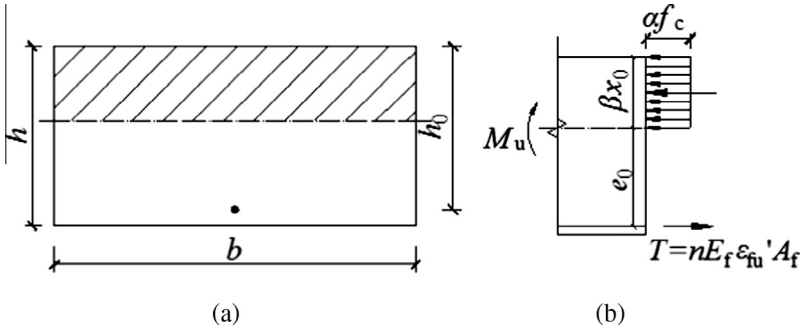

Fig. 19. Bending stress distribution of TRSSC beam section: (a) section of TRSSC beam and (b) section of equivalent stress.

Table 10
Comparison of the cracking and ultimate loads of the calculation and experimental results.

Specimen number	Cracking load			Ultimate load		
	Calculation result F^j_{cr}/KN	Experimental result F^s_{cr}/KN	F^j_{cr}/F^s_{cr}	Calculation result F^j_u/KN	Experimental result F^s_u/KN	F^j_u/F^s_u
S1-3-A	1.88	1.92	0.98	2.82	2.31	1.22
S2-3-A	1.69	1.44	1.17	2.87	2.23	1.28
S1-3-B	1.68	1.50	1.12	1.48	1.61	0.91
S2-3-B	1.54	1.46	1.05	1.46	1.52	0.96
S1-3-C	1.68	1.93	0.87	2.88	3.32	0.87
S2-3-C	1.61	1.80	0.89	2.90	3.64	0.79
C-3-A	0.85	0.95	0.89	2.95	2.30	1.28
S1-8-A	1.60	1.71	0.94	1.39	1.84	0.76
S2-8-A	1.47	1.34	1.10	1.38	1.70	0.81

$$M_{cr} = M_1 + M'_{cr} \tag{16}$$

where M_1 is the elimination pressure moment, M'_{cr} is the cracking moment of the non-self-stressing concrete beam, and M_1 is given by Eq. (17):

$$M_1 = \frac{f_{fu}\varepsilon}{\varepsilon_{fu}A_c}(1 + e_0)W \tag{17}$$

where f_{fu} is the ultimate load of fiber bundle, A_c is the section area of the beam, e_0 is the eccentricity, and W is the section resistance moment. The calculated cracking and ultimate moments are transformed into the corresponding cracking and ultimate loads (Table 10).

The theoretical calculation values of the cracking load are within an error range of 2–17% against the experimental values (Table 10). The theoretical calculation values of the ultimate load have an error range of 9–28% relative to the experimental values. The calculation values of the cracking load are generally much closer to the experimental values than to the ultimate load calculations. According to Eq. (17), the cracking load calculation values are related to the ε value, which is determined by the limited expansion ratio and has no relation with the plane section assumption. Therefore, the calculation and experimental values of the cracking load do not differ significantly. The plane section assumption is not established from the concrete cracking to the ultimate state. The fiber bundle is not broken at the same time, thereby causing the calculation and experimental values of the ultimate load to vary substantially.

4. Conclusions

The expansion of the self-stressing concrete improves the bond behavior between the textile and concrete, which increases the ultimate pull-out force and the energy dissipation capacity.

(1) The SEM test results indicate that the bond behavior between textile and self-stressing concrete is superior to that between textile and common concrete.
(2) The cracking load of the TRSSC sheet is related to the water cement ratio of self-stressing concrete, cover thickness, and distribution textile rate.
(3) The calculations of the cracking and the ultimate loads of TRSSC sheet must consider the force equilibrium and deformation geometric equations. This study proposes the calculation formula of the TRSSC elimination pressure moment, which is congruent with the experimental results.

Acknowledgement

Financial support of the work reported in this paper, by National Natural Science Foundation of China (Grant No. 51108207) and The State Key Program of National Natural Science of China (Grant No. 41430642), is gratefully acknowledged.

References

[1] F. Jess, M. Curbach, The present and the future of textile reinforced concrete, in: Fifth International Conference on Fiber-Reinforced Plastics for Reinforced Concrete Structures, Thomas Telford, London, 2001, pp. 593–605.
[2] J. Heggr, S. Voss, Investigations on the bearing behavior an application potential of textile reinforced concrete, Eng. Struct. 30 (7) (2008) 2050–2056.
[3] A. Brückner, R. Ortlepp, M. Curbach, Textile reinforced concrete for strengthening in bending and shear, Mater. Struct. 39 (2006) 741–748.
[4] M. Schleser, B. Walk-Lauffer, M. Raupach, et al., Application of polymers to textile-reinforced concrete, ASCE J. Mater. Civ. Eng. 18 (5) (2006) 670–676.
[5] Jianguo Dai, Chengkui Huang, Research on the basic mechanical properties of steel fiber reinforced self-stressing concrete, J. Build. Mater. 4 (1) (2001) 70–74.
[6] B. Wang, T. Man, H. Jin, Expansive and mechanical properties of textile reinforced self-stressing concrete, Constr. Build. Mater. 93 (2015) 1042–1050.
[7] Rabea Barhum, Viktor Mechtcherine, Effect of short, dispersed glass and carbon fibres on the behaviour of textile-reinforced concrete under tensile loading, Eng. Fract. Mech. 92 (2012) 56–71.
[8] Jens Hartig, Ulrich Haubler-Combe, Kai Schicktanz, Influence of bond properties on the tensile behavior of textile reinforced concrete, Cement Concr. Compos. 30 (2008) 898–906.
[9] Shilang Xu, He Li, Bond property and experimental methods of textile reinforced concrete, J. Wuhan Univ. Technol.-Mater 22 (3) (2007) 529–532.
[10] Yuxi Zhao, Weiliang Jin, Test study on bond stress-slip relationship of concrete and steel bar, J. Build. Struct. 23 (1) (2002) 32–37.
[11] A. Balarbi, D.N. Richardson, Effect of contamination on reinforcing bar concrete bond, J. Perform. Construct. Facil. 24 (3) (2010) 206–214.
[12] Wenwei Wang, Jianguo Dai, Self-stressed fiber reinforced concrete as negative moment connection for strengthening of multi-span simply-supported girder bridges, Adv. Struct. Eng. 16 (6) (2013) 1113–1127.
[13] Gao Xiangling, Jie Li, Theory and test on computative model of local bond strength between reinforcing bars and concrete, Build. Struct. 35 (4) (2005) 10–12.
[14] Xu Bingye, Liu Xinsheng, Application of Elastic and Plastic Mechanics, TsingHua University Press, Beijing, 1995. p. 9.
[15] B. Wang, T. Man, H. Jin, Prediction of expansion behavior of self-stressing concrete by artificial neural network and fuzzy inference system, Constr. Build. Mater. 84 (2015) 184–191.
[16] G. Papanicolaou Catherine, C. Papantoniou Ioannis, Mechanical behavior of textile reinforced concrete (TRC)/concrete composite elements, J. Adv. Concr. Technol. 8 (1) (2010) 35–47.
[17] W.W. Wang, Zhao Guofan, Huang Chengkui, An experimental study of strengthening of initially loaded reinforced concrete beams using CFRP sheets, Eng. Mech. 21 (4) (2004) 175–177.
[18] ACI 318R-08, Building Code Requirements for Structural Concrete and Commentary, American Concrete Institute, Farmington Hill, Mi, 2008.